Applied Physics Letters

Imprinting the complex dielectric permittivity of liquids into the spintronic terahertz emission

Cite as: Appl. Phys. Lett. **119**, 091104 (2021); https://doi.org/10.1063/5.0056909
Submitted: 15 May 2021 . Accepted: 13 August 2021 . Published Online: 31 August 2021

Vasileios Balos, Patrick Müller, Gerhard Jakob, Mathias Kläui, Mohsen Sajadi, et al.

Applied Physics Letters ARTICLE scitation.org/journal/apl

Imprinting the complex dielectric permittivity of liquids into the spintronic terahertz emission

Cite as: Appl. Phys. Lett. **119**, 091104 (2021); doi: 10.1063/5.0056909
Submitted: 15 May 2021 · Accepted: 13 August 2021 ·
Published Online: 31 August 2021

Vasileios Balos,[1] Patrick Müller,[1] Gerhard Jakob,[2] Mathias Kläui,[2] and Mohsen Sajadi[1,3,a)]

AFFILIATIONS

[1]Fritz Haber Institute of the Max Planck Society, 14195 Berlin, Germany
[2]Institute of Physics, Johannes Gutenberg University Mainz, 55099 Mainz, Germany
[3]Department of Chemistry, University of Paderborn, 33098 Paderborn, Germany

[a)]**Author to whom correspondence should be addressed:** sajadi@fhi-berlin.mpg.de

ABSTRACT

We report an approach in time-domain terahertz (THz) spectroscopy for measuring the dielectric response of liquids based on inherent properties of spintronic THz emitters (STEs). The THz electric field radiated from the STE is inversely proportional to the sum of the complex refractive indices of the media surrounding the thin metallic stack of the STE and the stack's conductivity. We demonstrate that by bringing a liquid in contact with the emitter, its complex refractive index and accordingly its dielectric response are imprinted into the radiated electromagnetic field from the emitter. We use water as the test liquid and ascertain its dielectric loss and permittivity in the range of ~0.3–15 THz.

Terahertz time-domain spectroscopy (THz-TDS) is a powerful technique for exploring low-energy excitations in solids,[1,2] rotational transitions of molecular gases,[3] and intermolecular dynamics of condensed molecular systems and liquids.[4–9] By employing short THz pulses and measuring their transmitted or reflected electric fields, THz-TDS enables direct access into the complex refractive index and the complex permittivity of matter.[10–13] For a relatively narrow spectral range, namely, from ~0.5 up to ~3 THz, commercial THz-TDS setups are available and routinely employed to measure the THz response of various systems.[10–15] However, this narrow frequency window is often insufficient to capture the entire collective motions and intermolecular dynamics of molecular liquids and other systems. For many interesting molecular liquids such as water, aqueous ionic solutions, and biological systems, the intermolecular dynamics cover an ultrabroad frequency range and extend beyond 10 THz. Despite significant progress,[16] technical challenges for the generation of ultrabroadband THz pulses limit the accessible THz frequency window within the reach of only one technique; hence multiple spectroscopic techniques are generally employed to measure the desired response over the entire THz window.[17]

Recently, a spintronic THz emitter (STE) was introduced,[18,19] whose radiation bandwidth is extremely large and covers the THz frequency window of ~0.3–30 THz continuously, surpassing the radiation bandwidth of traditional THz emitters such as photoconductive antennas[20] and electro-optic semiconductor crystals.[21,22] STE is a nanometers-thick metallic stack consisting of a ferromagnetic (FM) layer sandwiched between two nonmagnetic (NM) layers, where the in-plane magnetization of the FM layer is saturated by an external magnetic field. Upon excitation with a femtosecond laser pulse, electrons in the metallic stack gain kinetic energy and due to the different transport properties of the electrons in the FM and NM layers, a spin current along the laser propagation direction (z direction) is generated. In the FM layer, the majority spin-up electrons have significantly larger density, band velocity, and lifetime compared to those of the minority spin-down electrons.[23] As such, the spin-current is strongly spin-polarized,[24] and by crossing into the NM layer, the spin-up and -down electrons are deflected in opposite directions.[25,26] Accordingly, the spin-current in the z direction is converted into a net charge current in the xy plane. The latter in-plane current causes the radiation of a broad THz electromagnetic pulse, whose electric field is given by[18]

$$\hat{E}(\omega) = \frac{Z_0}{\hat{n}_1(\omega) + \hat{n}_2(\omega) + C} J_c(\omega), \tag{1}$$

where $J_c(\omega)$ is the in-plane charge-current, $\hat{n}_i(\omega)$, $i = 1, 2$ are the refractive indices of the media surrounding the metallic stack, and

$Z_0 \approx 377\,\Omega$ is the vacuum impedance and the parameter $C = Z_0\hat{G}$, where $\hat{G} = 7.78 \times 10^{-3}\,\Omega^{-1}$ is the conductance of the metallic stack,[27,28] obtained from THz transmission spectroscopy. Note that the in-plane current $J_c(\omega)$ causes the radiation of THz pulses along (and also opposite) the laser pulse propagation direction. As discussed below, this feature is essential for developing a spectroscopic technique based on the STE to resolve the ultrabroadband dielectric response of liquids.

To fully employ the broad radiative bandwidth of the STE for dielectric spectroscopy, one may recall the challenges with commonly used transmission and reflection THz-TDS approaches. In the transmission geometry, multiple internal reflections of the THz wave inside the media and their frequency-dependent complex refractive indices make the pattern of the transmitted THz waveform and accordingly its Fourier spectrum highly complicated to disentangle.[27] Although this difficulty is relieved in the reflection geometry, the amplitude of the THz signal is drastically reduced due to the transmission and the reflection losses at the surfaces of the THz-optical elements, consequently reducing the effective bandwidth of the measured THz response.

In this work, we take advantage of an inherent attribute of the STE, namely, the Fabry–Pérot interference of the THz pulse inside the metallic stack, to demonstrate an approach in THz-TDS by which we obtain the broadband dielectric response of liquids. As shown in Fig. 1, the metallic stack of the STE is sandwiched between two media, whose complex refractive indices strongly differ from that of a metal; hence, the radiated THz wave undergoes many internal reflections. As a result, the refractive indices of the surrounding media directly contribute to shaping the waveform of the emitted THz pulse. We use this effect to extract the complex refractive index of a liquid in contact with the metallic side of the STE. As given in Eq. (1), the emitted THz electric field is inversely proportional to the complex refractive indices of the surrounding media plus a constant that refers to the conductivity of the thin metallic stack. Therefore, by choosing diamond, whose refractive index is real and constant over the entire THz frequency range as the STE substrate[28] and by measuring the THz electric field, we determine the complex refractive index of a liquid in contact with its metallic side.

As a proof of principle, we obtain the complex dielectric permittivity and refractive index of liquid water. The intermolecular dynamics of water are ultrabroad and extend well beyond 10 THz. Moreover, because of its importance in various research disciplines, high quality dielectric data of water are available to which we can compare our results. For instance, using Fourier-transform infrared spectroscopy, optical constants of water in the far-infrared region were determined.[29–32] THz-TDS in reflection[33–35] and transmission[36–38] geometries has also been employed for measuring the low-frequency dielectric permittivity of water. More recently, high power laser sources were employed to generate THz pulses with ultrabroad spectral bandwidth. Using a THz-plasma source, Wang *et al.* performed THz-TDS and reported the ultrabroad dielectric response of water.[39] In another study, Folpini *et al.* used amplifier laser systems to generate intense THz pulses via optical rectification in an organic crystal and reported the ultrabroadband absorbance of water.[40,41] In the current work, we show the feasibility of measuring the ultrabroad dielectric response of liquids, such as water, with femtosecond oscillator laser systems.

The schematic of the experiment is illustrated in Fig. 1. A short laser pulse (∼10 nJ pulse energy, ∼20 fs duration, 80 MHz repetition rate at 800 nm central wavelength) generated by a Ti:sapphire oscillator is split by a ratio of 80:20 as the pump and probe pulses, respectively. The pump laser pulse is focused by an off-axis parabolic mirror

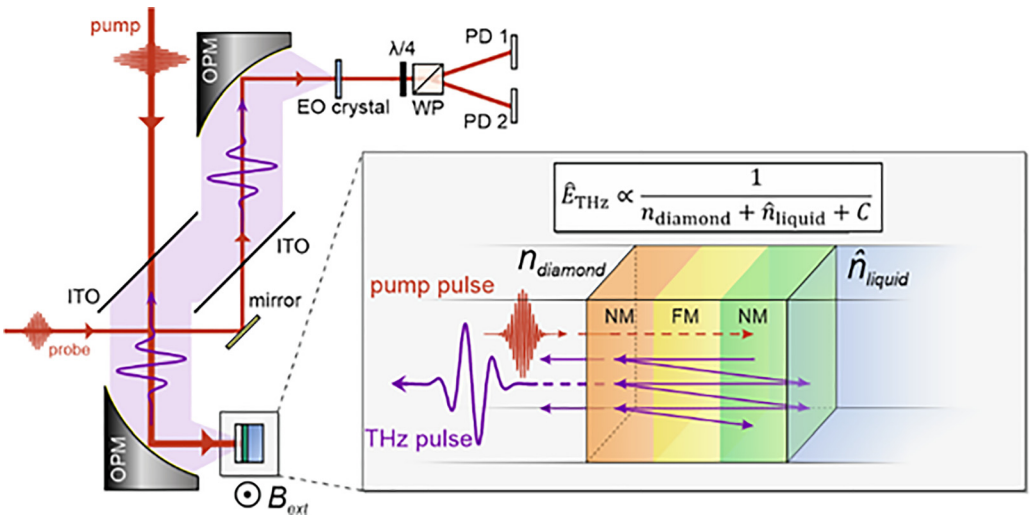

FIG. 1. Schematic of the THz time-domain spectroscopy setup based on unique inherent features of the STE. A femtosecond laser pulse with ∼1.5 nJ energy is focused by an off-axis parabolic mirror (OPM) on the STE from its diamond side. The backward THz emission of the STE is collected and collimated by the same OPM and reflected to the second OPM with two indium tin oxide (ITO) coated glass slides to be focused on the electroptic (EO) medium. The transient THz electric field is resolved by measuring the induced ellipticity of an optical probe pulse, using a quarter waveplate ($\lambda/4$), a Wollaston prism (WP), and two balanced photodiodes (PDs). A static magnetic field of 10 mT magnetizes the feromagnetic (FM) layer of the STE. The enlarged box shows the FM of the STE sandwiched between two nonmagnetic (NM) layers. The waveform of the emitted THz pulse is affected by the refractive indices of the surrounding media, diamond, and water via multiple internal reflection of the THz pulse inside the metalic stack.

(OPM, reflective focal length $f = 2$ in.) on the STE from its diamond side. The emitted THz radiation in the backward direction (from the diamond side) is collimated by the same OPM and guided by two indium tin oxide (ITO) plates to the second OPM ($f = 2''$) and focused on an electro-optic medium.

The probe pulse is delayed by an oscillating retroreflector (frequency of 5 Hz) for sampling the THz wave by means of the electro-optic sampling (EOS) technique.[42,43] As the EOS media, we use a 250 μm thick gallium phosphide (GaP, 110 cut) crystal to cover frequencies up to ~7 THz and a 10 μm thick ZnTe (110 cut) crystal to cover frequencies up to 15 THz. The thin ZnTe crystal is attached to a 300 μm thick THz-inactive ZnTe crystal for stability. The liquid cell is built on the metallic rear side of the STE, which is constructed by sputter deposition of 2.0 nm thick tungsten (first NM layer), 1.8 nm $Co_{20}Fe_{60}B_{20}$ (FM layer), and 2.0 nm thick platinum (second NM layer) on 1.2 mm thick polycrystalline diamond. We use ultrapure liquid water (Milli-Q from MILLIPORE Q-POD) as our testing liquid. To make a direct comparison between the dielectric response of water obtained with this approach and that obtained with an established method, we developed a reflection THz-TDS implemented in the same experimental setup, see the supplementary material and Fig. S1. All measurements are performed inside a box purged with nitrogen.

The THz signals from the STE with and without water on its rear side (hereafter called sample and reference signals, respectively) measured with the GaP and the thin ZnTe crystals are shown in Figs. 2(a) and 2(c). The reference and sample signals bear large and clearly distinguishable amplitudes. The latter difference is more pronounced in the Fourier spectra of the pulses, see Figs. 2(b) and 2(d). In the Fourier domain, we have determined the dynamic range (DNR) of our signals as well. As shown in Fig. S2, DNR reaches ~40 and ~30 dB in the GaP and ZnTe measurements, respectively. The phase shifts of the sample signals relative to the reference signal phase are shown in the upper panel of Figs. 2(b) and 2(d). In both cases, the absolute value of the phase shift decreases with increasing frequency.

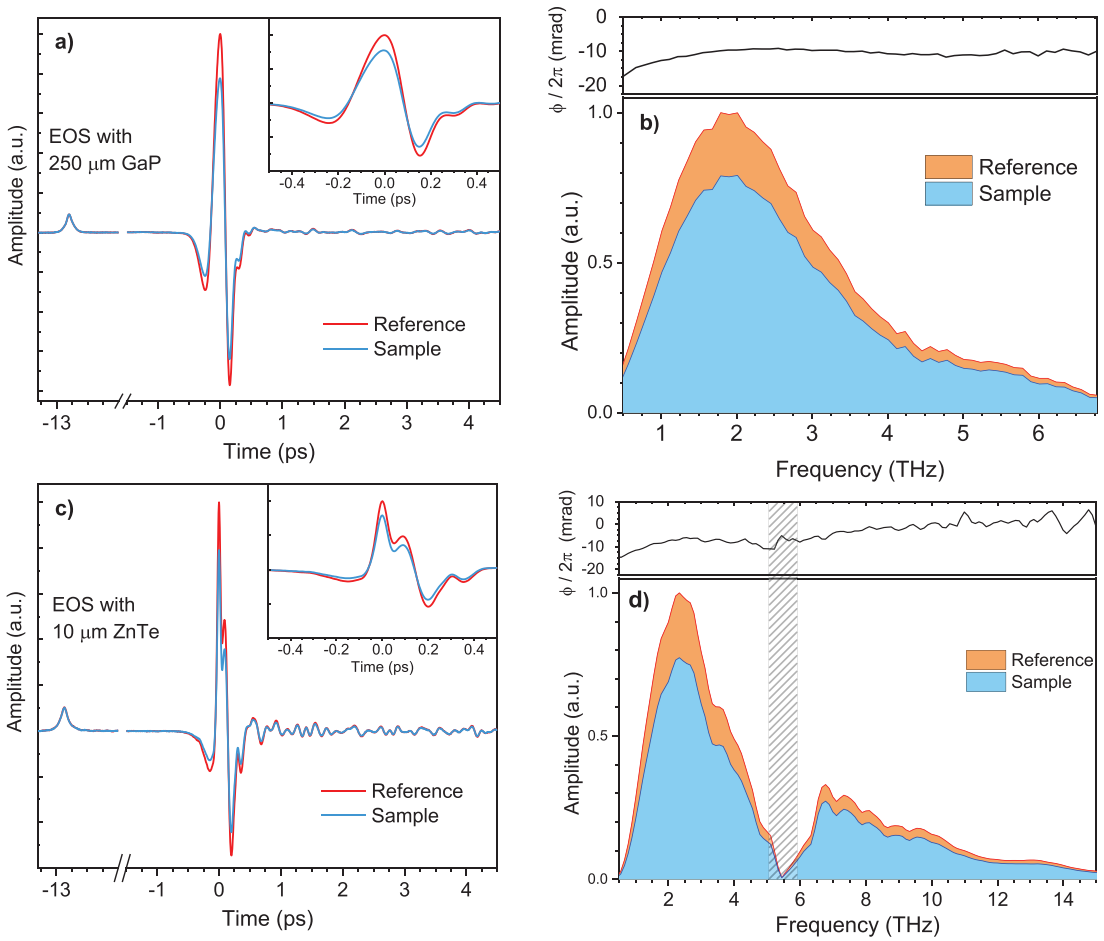

FIG. 2. THz emissions from the STE. (a) THz electric fields with (blue line) and without (red line) water on the rear side of STE, measured with 250 μm GaP as the EOS medium. (b) Amplitude spectra of the reference and sample signals. The upper panel shows the phase difference between the sample and reference signals. (c) and (d) As in panels (a) and (b), measured with 10 μm ZnTe. The measured signals with the ZnTe crystal are subjected to a Norton–Beer apodization (FWHM = 2.0) (for details, see Ref. 53). The signals at around −13 ps in panels (a) and (c) are the phase markers (see the text for details). The dashed area in panel (d) indicates the Reststrahlen-band around 5.5 THz in the ZnTe crystal.

Note that, although the phase shift of the THz pulse upon introducing the liquid on the STE's rear side is small, the high signal-to-noise ratio of the STE signals allows measuring the small phase shifts with high accuracy. The THz waves measured with the thin ZnTe crystal are almost five times weaker than those measured with the GaP crystal, due to its lower thickness. The shaded area in Fig. 2(d) around 5.5 THz marks the frequency range that is affected by the Reststrahlen-band in the ZnTe crystal.[44] The feature around the time delay equal to −13 ps is the phase marker, and as described below, it is devised to lock the mechanical phase fluctuations of the THz pulses. The phase marker results from the third-order nonlinear optical Kerr effect (OKE) response of the EOS crystal induced by the back-reflected pump pulse from the air–diamond interface. As the 800 nm pulse is reflected from the same diamond that the STE is deposited on and propagates along the same path that THz pulse travels to, its induced instantaneous electronic OKE signal carries all mechanical phase fluctuations and laser drifts that are also modulated on the THz pulse. As a result, the temporal position of the THz pulses can be corrected with the accuracy on the same order as the cross correlation of the optical pump and the probe pulses, i.e., ∼20 fs. For the selected 1.2 mm thick diamond, the OKE signal appears at −20 ps (relative to the THz pulse position) and its first echo signal at −13 ps, as shown in Fig. 2. Note that the time delay of the latter echo signal matches the thickness of the indium tin oxide (ITO) coated glass slides.

After performing the phase correction, we calculate the complex refractive index of water $\hat{n}_w$ by forming the ratio between the sample $\hat{E}_s(\omega)$ and reference $\hat{E}_r(\omega)$ complex field amplitudes using Eq. (1)

$$\frac{\hat{E}_s(\omega)}{\hat{E}_r(\omega)} = \frac{\left|\hat{E}_s(\omega)\right|}{\left|\hat{E}_r(\omega)\right|} e^{i\varphi(\omega)} = \frac{n_{\mathrm{dia}} + 1 + Z_0\hat{G}(\omega)}{n_{\mathrm{dia}} + \hat{n}_w + Z_0\hat{G}(\omega)}, \tag{2}$$

where n_{dia} is the refractive index of the diamond and $\varphi(\omega)$ is the phase shift of the sample signal relative to that of the reference signal. Solving this equation for $\hat{n}_w$, we obtain

$$\hat{n}_w(\omega) = A\frac{\left|\hat{E}_r(\omega)\right|}{\left|\hat{E}_s(\omega)\right|} e^{-i\varphi(\omega)} - B, \tag{3}$$

where $A = 1 + n_{\mathrm{dia}} + Z_0\hat{G}$ and $B = A - 1$.

The real part of $\hat{n}_w(\omega) = n(\omega) + i\kappa(\omega)$ is indeed the refractive index, and its imaginary part is related to the absorption coefficient via $\alpha(\omega) = 4\pi\frac{\kappa(\omega)}{\lambda}$, with λ being the wavelength of light. Therefore, the latter two quantities are obtained

$$n(\omega) = A\frac{\left|\hat{E}_r(\omega)\right|}{\left|\hat{E}_s(\omega)\right|}\cos\varphi(\omega) - B, \tag{4a}$$

$$\alpha(\omega) = -\frac{4\pi}{\lambda}A\frac{\left|\hat{E}_r(\omega)\right|}{\left|\hat{E}_s(\omega)\right|}\sin\varphi(\omega). \tag{4b}$$

The real and imaginary components of the complex refractive index are also related to the complex dielectric permittivity through $\hat{\varepsilon}(\omega) = \varepsilon'(\omega) + i\varepsilon''(\omega) = \hat{n}_w(\omega)^2$;[45] hence, the dielectric permittivity $\varepsilon'(\omega)$ and loss $\varepsilon''(\omega)$ can be determined

$$\varepsilon'(\omega) = A^2\frac{\left|\hat{E}_r(\omega)\right|^2}{\left|\hat{E}_s(\omega)\right|^2}\cos 2\varphi(\omega) - 2AB\frac{\left|\hat{E}_r(\omega)\right|}{\left|\hat{E}_s(\omega)\right|}\cos\varphi(\omega) + B^2, \tag{5a}$$

$$\varepsilon''(\omega) = -A^2\frac{\left|\hat{E}_r(\omega)\right|^2}{\left|\hat{E}_s(\omega)\right|^2}\sin 2\varphi(\omega) + 2AB\frac{\left|\hat{E}_r(\omega)\right|}{\left|\hat{E}_s(\omega)\right|}\sin\varphi(\omega). \tag{5b}$$

Next, we use Eqs. (4) and (5) and the spectral amplitudes and phase shifts shown in Fig. 2 to determine $\varepsilon'(\omega)$, $\varepsilon''(\omega)$, $n(\omega)$, and $\alpha(\omega)$ of water. The results are shown in Fig. 3 and demonstrate the broad dielectric response of water determined in the range of ∼0.3–7 THz.

It is important to note that by introducing the liquid on the STE's metallic rear side, the optical pump absorption by the STE metallic stack slightly reduces, which causes an amplitude drop in the emitted THz pulse. As this effect only influences the amplitude of the THz signal, we can correct it by implementing a scaling factor, i.e., $\left|\hat{E}_s(\omega)\right| = f^{-1}\left|\hat{E}_{s,m}(\omega)\right|$, where $\left|\hat{E}_s(\omega)\right|$ is the THz spectrum after the amplitude correction and $\left|\hat{E}_{s,m}(\omega)\right|$ is the original THz spectrum displayed in Figs. 2(b) and 2(d). We determine this factor by comparing the dielectric loss amplitude of water obtained via Eq. (4) with the same quantity measured with the reflection cell approach. Following both procedures, the scaling factor equals $f = 0.93$. Note that f can

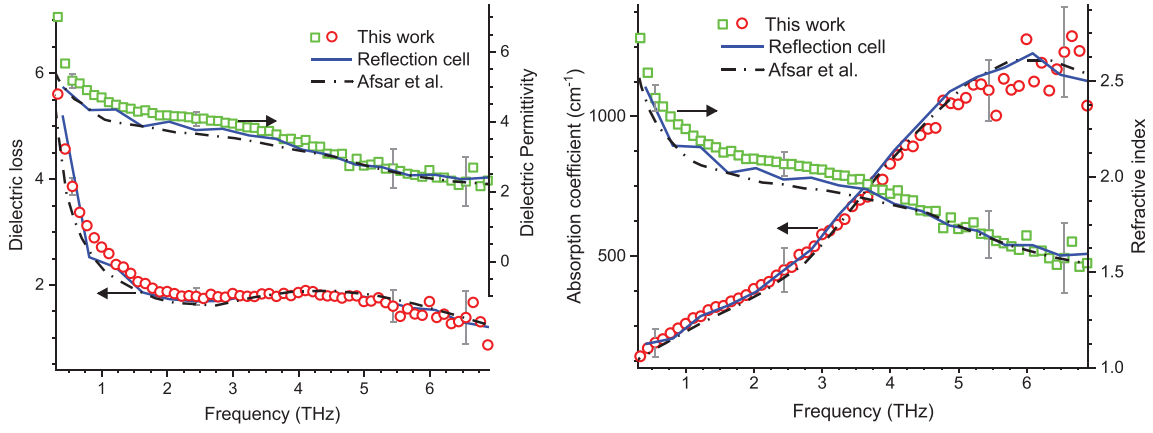

FIG. 3. Left, dielectric loss and permittivity of water obtained by the STE THz emission according to Eq. (5). Right, absorption coefficient and refractive index of water obtained according to Eq. (4). The STE results are compared with the measurement results from the silicon reflection cell and with the results from Ref. 31. The error bars indicate the standard deviation between the results from three consecutive scans, see Fig. S3.

also be determined by comparing the STE's light absorption with and without the liquid on its rear side.

We also compare the complex dielectric and refractive index obtained via Eqs. (4) and (5) with those reported in the work by Afsar and Hasted[31] and also our own measurement with the reflection cell. As shown in Fig. 3, the agreement among the latter three results proves the soundness of extracting the superimposed dielectric response of liquids in contact with the STE from its radiated THz pulse. Additionally, we provide a comparison with more reference data in Figs. S5–S7 for completeness.[17,29,46]

Although the extracted complex dielectric and refractive index data of water up to ∼7 THz are already a considerable achievement, we further exploit the broad STE emission bandwidth and extend the extraction of the complex dielectric and refractive index of water beyond 10 THz. To this end, we analyze the results obtained with the thin ZnTe crystal. The latter crystal has a very broad THz response, extending far beyond 10 THz with only a narrow Reststrahlen-band around 5.5 THz.[44] Using Eqs. (4) and (5), we calculate the complex refractive index and permittivity of water in the range ∼0.3–15 THz. As displayed in Fig. 4 (left panel), while $\varepsilon'(\omega)$ matches well with the results of Ref. 31, $\varepsilon''(\omega)$ deviates from the same reference at high frequencies. Note also that the drop in the amplitude of the THz signals at high frequencies hinders the use of the reflection cell approach to obtain $\varepsilon(\omega)$ above ∼7 THz.

The ability to determine $\varepsilon'(\omega)$ and $n(\omega)$ but not $\varepsilon''(\omega)$ and $\alpha(\omega)$ may be explained by the relation of these quantities to the absolute value of the phase shift $\varphi(\omega)$. As shown in Figs. 2(b) and 2(d), the absolute value of the phase shift $\varphi(\omega)$ decreases by increasing frequency, which is due to the increase in absorption and accordingly decreases in the penetration depth of the THz pulse into the water layer on the rear side of the STE. Analytically in accord with Eq. (5) [same holds for Eq. (4) too], the variation of $\varepsilon'(\omega)$ with respect to φ becomes small when φ approaches zero, i.e., $\frac{d\varepsilon'(\omega)}{d\varphi(\omega)}|_{\varphi\to 0} \approx 0$, while $\frac{d\varepsilon''(\omega)}{d\varphi(\omega)}|_{\varphi\to 0}$ approaches its maximum value. As a result, $\varepsilon''(\omega)$ is highly sensitive to phase fluctuations of the THz pulses at higher frequencies, whereas $\varepsilon'(\omega)$ suffers much less from such fluctuations.

In order to obtain the ultrabroadband dielectric loss $\varepsilon''(\omega)$ from our results, we use the fact that $\varepsilon''(\omega)$ and $\varepsilon'(\omega)$ are connected via the Kramers–Kronig relation;[47–49] hence, by subjecting $\varepsilon'(\omega)$ to the Kramers–Kronig transform, we calculate $\varepsilon''(\omega)$, following the procedure given in Ref. 50 and references therein. As shown in Fig. 4, the calculated $\varepsilon''(\omega)$ via the Kramers–Kronig transformation matches well with the reference data from Ref. 31. Note that, the mechanical phase fluctuation and accordingly our dependence on using the Kramers–Kronig relation to obtain $\varepsilon''(\omega)$ beyond ∼7 THz can be mitigated by the miniaturization of the experimental setup and using micro-cavities to hold the sample. The latter modifications go beyond the scope of this work and will be addressed in a forthcoming publication. We obtain $\alpha(\omega)$ via the relation between $\hat{\varepsilon}(\omega) = \hat{n}_w(\omega)^2$, see also Ref. 36.

In conclusion, we demonstrated an approach in time-domain THz spectroscopy to obtain ultrabroadband complex dielectric permittivity of liquids using femtosecond oscillator laser systems. This approach is based on inherent properties of the spintronic THz emitter, according to which the complex refractive indices of the surrounding media of the emitter are imprinted on its THz emission. Using water as our testing sample, we obtained its complex dielectric permittivity and refractive index in the range of ∼0.3–15 THz, for which otherwise a few methods need to be combined to obtain the same information.[17] By miniaturization of the spectrometer, the phase fluctuation of the STE emission will drastically be reduced; hence, the accessible THz bandwidth and its accuracy will increase.

In addition to ultrabroadband THz spectroscopy of liquids with fs-oscillator laser systems, the unique features of the STE offer opportunities to employ THz spectroscopy in new applications. For instance, (i) as the interaction volume of the THz-sample is very small (determined by the laser spot on the STE and the penetration depth of the THz inside the sample), one can study samples with microliter volume; crucial in THz spectroscopy of biological systems. (ii) Spectroelectrochemistry

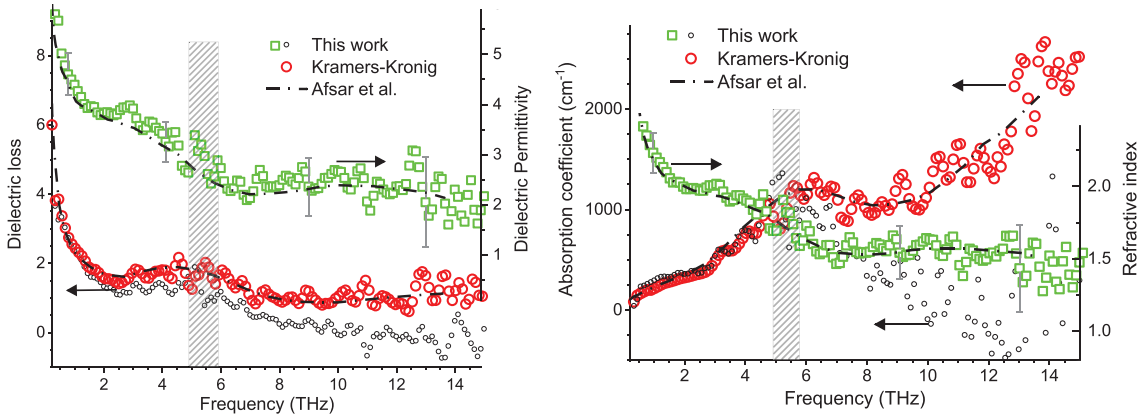

FIG. 4. Left, dielectric loss and permittivity of water. Right, absorption coefficient and refractive index of water. Using a thin ZnTe crystal as the EO medium, we obtain the dielectric response of water in the frequency interval of ∼0.3–15 THz via the STE emission approach [see Eq. (4)]. While $\varepsilon'(\omega)$, (green squares) agrees well with the result of Afsar and Hasted (dashed-dotted line, Ref. 31), $\varepsilon''(\omega)$ (empty-black circles) deviates from this reference, due to the dominance of the impacts of the phase fluctuations and laser drifts at the high frequency part of the displayed signals. The calculated $\varepsilon''(\omega)$ (empty-red circles) via the Kramers–Kronig transform of $\varepsilon'(\omega)$, however, matches well with the reference $\varepsilon''(\omega)$ obtained from Afsar and Hasted.[31] To obtain the absorption coefficient, we have used data in the left panel and the relation $\hat{\varepsilon}(\omega) = \hat{n}_w(\omega)^2$. The dashed areas mark the Reststrahlen-band of the ZnTe crystal around 5.5 THz. The error bars indicate the standard deviation between the results from three consecutive scans, see Fig. S4.

can be facilitated at THz frequencies, where the metallic stack of the emitter plays the role of the cathode, offering the opportunity for *in situ* THz-TD electrochemical spectroscopy and easing the challenges in construction of THz-transparent electrochemical cells.[51] Moreover, (iii) the miniaturization of the STE may pave the way for fabricating THz endoscopes for screening diseases that involve molecular processes with clear THz signatures, e.g., DNA methylation in cancer cells.[52]

See the supplementary material for THz-TDS in reflection geometry and additional results.

We thank Genaro Bierhance for his salient contribution in performing experiments and analyzing the results under the supervision of M.S. We also wish to thank Tobias Kampfrath for fruitful discussions. Funding from H2020 FET-OPEN project ASPIN (Grant No. 766566) is acknowledged by V.B., G.J., and M.K. Moreover, G.J. and M.K. acknowledge that this project has received funding from the European Union's Horizon 2020 research and innovation programme under Grant Agreement No. 863155 (s-Nebula) and the DFG (SFB TRR 173 Spin+X Project No. A01 268565370).

DATA AVAILABILITY

The data that support the findings of this study are available from the corresponding author upon reasonable request.

REFERENCES

[1]D. E. Mittleman, *Sensing with Terahertz Radiation* (Springer, Berlin, 2003).
[2]A. V. Kimel, A. M. Kalashnikova, A. Pogrebna, and A. K. Zvezdin, Phys. Rep. **852**, 1–46 (2020).
[3]D. M. Mittleman, R. H. Jacobsen, R. Neelamani, R. G. Baraniuk, and M. C. Nuss, Appl. Phys. B **67**, 379 (1998).
[4]D. A. Schmidt, S. Funkner, B. P. Born, R. Gnanasekaran, G. W. Schwaab, D. M. Leitner, and M. Havenith, J. Am. Chem. Soc. **131**, 18512 (2009).
[5]P. Schienbein, G. Schwaab, H. Forbert, M. Havenith, and D. Marx, J. Phys. Chem. Lett. **8**, 2373 (2017).
[6]U. Kaatze and Y. Feldman, Meas. Sci. Technol. **17**, R17 (2006).
[7]V. Balos, H. Kim, M. Bonn, and J. Hunger, Angew. Chem., Int. Ed. **55**, 8125 (2016).
[8]V. Balos, M. Bonn, and J. Hunger, Phys. Chem. Chem. Phys. **17**, 28539 (2015).
[9]G. Schwaab, F. Sebastiani, and M. Havenith, Angew. Chem., Int. Ed. **58**, 3000 (2019).
[10]K. Tielrooij, N. Garcia-Araez, M. Bonn, and H. J. Bakker, Science **328**, 1006 (2010).
[11]A. Stoppa, A. Nazet, R. Buchner, A. Thoman, and M. Walther, J. Mol. Liq. **212**, 963 (2015).
[12]V. Balos, M. Bonn, and J. Hunger, Phys. Chem. Chem. Phys. **19**, 9724 (2017).
[13]T. Fukasawa, T. Sato, J. Watanabe, Y. Hama, W. Kunz, and R. Buchner, Phys. Rev. Lett. **95**, 197802 (2005).
[14]J. Hunger, A. Stoppa, A. Thoman, M. Walther, and R. Buchner, Chem. Phys. Lett. **471**, 85 (2009).
[15]V. Balos, S. Imoto, R. R. Netz, M. Bonn, D. J. Bonthuis, Y. Nagata, and J. Hunger, Nat. Commun. **11**, 1611 (2020).
[16]H. G. Roskos, M. D. Thomson, M. Kreß, and T. Löffler, Laser Photonics Rev. **1**, 349 (2007).
[17]H. Yada, M. Nagai, and K. Tanaka, Chem. Phys. Lett. **464**, 166 (2008).
[18]T. Seifert, S. Jaiswal, U. Martens, J. Hannegan, L. Braun, P. Maldonado, F. Freimuth, A. Kronenberg, J. Henrizi, I. Radu, E. Beaurepaire, Y. Mokrousov, P. M. Oppeneer, M. Jourdan, G. Jakob, D. Turchinovich, L. M. Hayden, M. Wolf, M. Münzenberg, M. Kläui, and T. Kampfrath, Nat. Photonics **10**, 483 (2016).
[19]T. Seifert, S. Jaiswal, M. Sajadi, G. Jakob, S. Winnerl, M. Wolf, M. Kläui, and T. Kampfrath, Appl. Phys. Lett. **110**, 252402 (2017).
[20]J. E. Pedersen, V. G. Lyssenko, J. M. Hvam, P. U. Jepsen, S. R. Keiding, C. B. Sorensen, and P. E. Lindelof, Appl. Phys. Lett. **62**, 1265 (1993).
[21]X. C. Zhang, Y. Jin, and X. F. Ma, Appl. Phys. Lett. **61**, 2764 (1992).
[22]Q. Wu and X. C. Zhang, Appl. Phys. Lett. **67**, 3523 (1995).
[23]V. P. Zhukov, E. V. Chulkov, and P. M. Echenique, Phys. Rev. B **73**, 125105 (2006).
[24]M. Battiato, K. Carva, and P. M. Oppeneer, Phys. Rev. Lett. **105**, 027203 (2010).
[25]E. Saitoh, M. Ueda, H. Miyajima, and G. Tatara, Appl. Phys. Lett. **88**, 182509 (2006).
[26]D. Wei, M. Obstbaum, M. Ribow, C. H. Back, and G. Woltersdorf, Nat. Commun. **5**, 3768 (2014).
[27]J. Neu and C. A. Schmuttenmaer, J. Appl. Phys. **124**, 231101 (2018).
[28]A. J. Gatesman, R. H. Giles, G. C. Phillips, J. Waldman, L. P. Bourget, and R. Post, MRS Online Proc. Libr. **162**, 285 (1989).
[29]H. R. Zelsmann, J. Mol. Struct. **350**, 95 (1995).
[30]J. E. Bertie and Z. Lan, Appl. Spectrosc. **50**, 1047 (1996).
[31]M. N. Afsar and J. B. Hasted, J. Opt. Soc. Am. **67**, 902 (1977).
[32]I. Bergonzi, L. Mercury, J. B. Brubach, and P. Roy, Phys. Chem. Chem. Phys. **16**, 24830 (2014).
[33]L. Thrane, R. H. Jacobsen, P. Uhd Jepsen, and S. R. Keiding, Chem. Phys. Lett. **240**, 330 (1995).
[34]C. Rønne, P.-O. Åstrand, and S. Keiding, Phys. Rev. Lett. **82**, 2888 (1999).
[35]U. Møller, D. G. Cooke, K. Tanaka, and P. U. Jepsen, J. Opt. Soc. Am. B **26**, A113 (2009).
[36]J. T. Kindt and C. A. Schmuttenmaer, J. Phys. Chem. **100**, 10373 (1996).
[37]N. Q. Vinh, M. S. Sherwin, S. J. Allen, D. K. George, A. J. Rahmani, and K. W. Plaxco, J. Chem. Phys. **142**, 164502 (2015).
[38]J. Zhou, X. Rao, X. Liu, T. Li, L. Zhou, Y. Zheng, and Z. Zhu, AIP Adv. **9**, 035346 (2019).
[39]T. Wang, P. Klarskov, and P. U. Jepsen, IEEE Trans. Terahertz Sci. Technol. **4**, 425 (2014).
[40]G. Folpini, T. Siebert, M. Woerner, S. Abel, D. Laage, and T. Elsaesser, J. Phys. Chem. Lett. **8**, 4492 (2017).
[41]C. Somma, G. Folpini, J. Gupta, K. Reimann, M. Woerner, and T. Elsaesser, Opt. Lett. **40**, 3404 (2015).
[42]M. Tonouchi, Nat. Photonics **1**, 97 (2007).
[43]B. Ferguson and X. Zhang, Nat. Mater. **1**, 26 (2002).
[44]T. Kampfrath, J. Nötzold, and M. Wolf, Appl. Phys. Lett. **90**, 231113 (2007).
[45]A. Kremer and F. Schönals, *Broadband Dielectric Spectroscopy* (Springer, 2003).
[46]W. J. Ellison, J. Phys. Chem. Ref. Data **36**, 1 (2007).
[47]J. E. Bertie and Z. Lan, J. Chem. Phys. **105**, 8502 (1996).
[48]K. Shiraga, T. Suzuki, N. Kondo, and Y. Ogawa, J. Chem. Phys. **141**, 235103 (2014).
[49]K. Shiraga, Y. Ogawa, K. Tanaka, T. Arikawa, N. Yoshikawa, M. Nakamura, K. Ajito, and T. Tajima, J. Phys. Chem. B **122**, 1268 (2018).
[50]K. Shiraga, K. Tanaka, T. Arikawa, S. Saito, and Y. Ogawa, Phys. Chem. Chem. Phys. **20**, 26200 (2018).
[51]C. T. Nemes, J. R. Swierk, and C. A. Schmuttenmaer, Anal. Chem. **90**, 4389 (2018).
[52]J. H. Son, S. J. Oh, and H. Cheon, J. Appl. Phys. **125**, 190901 (2019).
[53]D. A. Naylor and M. K. Tahic, J. Opt. Soc. Am. A **24**, 3644 (2007).